This paper has bee published in International Journal of Rock Mechanics and Mining Sciences, 70, 400-406, doi:10.1016/j.ijrmms.2014.05.012.

Time-dependent brittle creep as a mechanism for time-delayed wellbore failure

Martin Schoenball*[1], David P. Sahara[1], and Thomas Kohl[1]

[1]*Karlsruhe Institute of Technology, Institute of Applied Geosciences, Karlsruhe, Germany*

Abstract

By drilling a wellbore cavity, high stresses arise at the wellbore wall, leading to the formation of breakouts which enlarge the hole to an elongated shape oriented along the direction of the minimum principal stress. If formation of breakouts is delayed, rock debris falls on the drill bit which may lead to stuck pipe problems or even abandonment of the drill string. Reasons for such time-delayed failure of the wellbore may be due to chemical fluid-rock interaction, especially in swelling clays. However, such delayed instabilities have also been observed e.g. in gneiss formations at the KTB borehole (Germany) that are not known to exhibit a swelling behavior. We propose to explain observations of delayed wellbore failure by time-dependent brittle creep, which has been observed for many types of rocks. Following this approach, rock fails under loads less than their short-time strength but after a long enough time span. This time is in exponential relation to the load applied to the rock. We implement a model developed for the creation of shear bands on the basis of time-dependent brittle creep by Amitrano and Helmstetter (2006). Here, progressive damage of the formation is captured by a damage parameter D and the time-to-failure TTF. Young's modulus E is decreased by a factor every time TTF is expired, i.e. when failure is reached. Subsequently, stresses are redistributed according to the new distribution of E in the formation. Using this approach, we obtain closure of the well with primary and secondary creep phases. Wellbore breakouts are formed progressively with deepening and widening of the initially damaged zone. After a certain time the formation of breakouts comes to an end with an Omori-like decay of failure approaching a steady-state.

*martin.schoenball@kit.edu

1 Introduction

Analysis of the stability of underground excavations is a standard engineering task for the construction of boreholes, tunnels and mining shafts. Such man-made cavities perturb the local stress field tremendously, potentially leading to different kinds of rock failure. Besides the safety aspects of controlling rock failure, stability problems are a major cost factor for the creation of underground cavities. To prevent such problems, it is necessary to calculate the stress and displacement fields around artificial cavities to plan for adequate measures in order to prevent excessive failure of the rock. Stresses around a wellbore orthogonal to principal stresses were derived in the classical paper by Kirsch (1898). Solutions for a more general case for inclined wellbores have been derived by Hiramatsu and Oka (1968). At the wellbore wall, compressive stresses reach a maximum in the direction of minimal principal stress, leading to the formation of breakouts. Excessive breakouts can be an obstacle for the further drilling process, as e.g. material may fall on the drill bit leading to stuck pipe problems, which delays the drilling progress or may even end in the abandonment of the drill string and the wellbore. Besides, breakouts forming at the wellbore wall are used to determine the stress state of the crust. As breakouts in a vertical wellbore form in the direction of minimum horizontal stress, breakouts can be used to determine the orientation of the tectonic stress tensor. Zoback et al. (1985, 2003) show breakout growth in depth, but no growth in width is observed in their numerical simulations. This forms the basis to use breakouts as stress indicators for stress magnitudes by determination of breakout geometry and width (Vernik et al., 1992; Brudy et al., 1997; Haimson and Chang, 2002). The previously mentioned studies use an elastic approach and a time-independent failure criterion to calculate the formation of breakouts. These approaches yield breakouts with a round shape. However, in laboratory experiments and in-situ V-shaped breakouts are frequently found (Lee and Haimson, 1993; Haimson, 2007; Zang and Stephansson, 2010). Zoback et al. (1985) describe the growth of breakouts at depth using elastic solutions applied to iteratively generated geometries of the wellbore cross-section including the breakout. However, they lack to answer the question why breakout growth at depth stops at some point, but already point to inelastic effects necessary for a stabilization of breakouts.

There is ample evidence for time-dependent evolution of breakouts (Triantafyllidis et al., 2010). Through repeated logging runs several examples of time-dependent breakout formation have been found. At KTB-VB scientific wellbore caliper logs were run 74 times over a period of over a year, making it possible to study time-dependent formation of breakouts at depths of 500 to 3000 m where the well advanced in gneiss and amphibolite rocks (Kessels, 1989). For several depth intervals growth of breakouts within the first 20 to 100 days after drilling was observed, followed by stabilization and cessation of breakout growth (Figure 1). At the Soultz geothermal project no breakouts were observed in the granite formation immediately after drilling, but after 1 year extensive breakouts had formed (Cornet et al., 2007). More recently, IODP scientific wells in muddy sediments south of Japan showed a time-dependent growth of

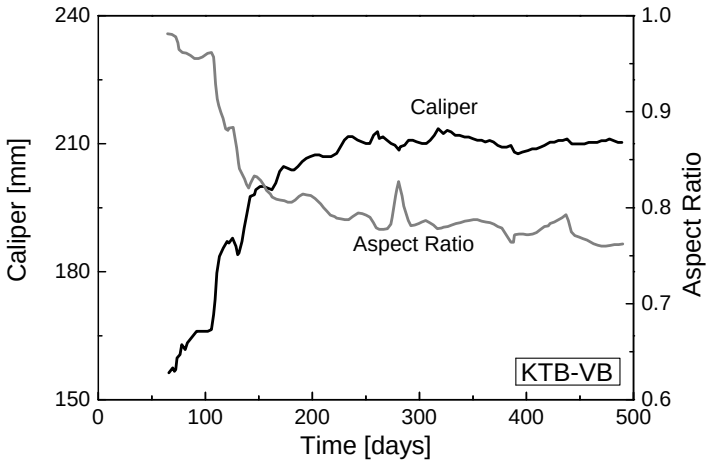

Figure 1: Caliper and ellipticity of well KTB-VB at the depth section 575-600 m obtained from 74 caliper runs showing the evolution of breakouts with time (modified from Kessels, 1989).

breakouts (Moore et al., 2011).

Haimson (2007) describes the micromechanical processes of breakout formation as observed for different rock types in laboratory experiments. Possible mechanisms for time-dependent mechanical behavior are chemical interaction, most notable in clayey formations (Chen et al., 2003), or in the form of stress solution at crack tips (Rutter, 1976), diffusion of pore fluid pressure (Detournay and Cheng, 1988), thermal stresses and mechanical creep. The latter mechanism is subject of this study and is treated by the principle of time-dependent brittle creep as a consequence of e.g. subcritical crack growth or stress corrosion (Anderson and Grew, 1977; Scholz, 1968; Das and Scholz, 1981; Atkinson, 1984; Brantut et al., 2013). Lockner (1998) experimentally derived a generalized law for the behavior of Westerly granite under general loading conditions. Using this law, he simulates time-dependent brittle creep with numerical methods. Amitrano and Helmstetter (2006) and Xu et al. (2012) model time-dependent brittle creep of 2D samples using the finite element method and explicit implementation of a time-to-failure law in the constitutive relations. They are able to numerically simulate e.g. creep strain curves and failure event rates that fit those of lab experiments very well. (Gran et al., 2012) use a block-slider model to simulate seismicity sequences. Specifically, to introduce the decaying activity of aftershock sequences, he introduces a time-to-failure approach. Within a certain parameter range, they obtain an event rate scaling conforming to Omori's law.

In this paper we combine a wellbore stress analysis with the numerical approach developed by Amitrano and Helmstetter (2006) in order to study the

temporal evolution of breakouts. For this, we develop a finite element simulator for the problem of an arbitrarily oriented wellbore and implement the time-to-failure approach, incorporating effective elastic moduli. We propose to link the damage at the wellbore wall to Young's modulus by a linear relation between damage and Young's modulus as in Amitrano and Helmstetter (2006) but test also two different relations. We study the temporal evolution of breakout growth, as well of the shape of the breakouts and compare it with laboratory studies.

2 Time-Dependent Brittle Creep

When rocks are subjected to high loads, but below their short-term strength they begin to creep. If the load is large enough, they show a trimodal behavior: the primary creeping phase is marked by a relatively high strain rate leveling off to a minimum value before it increases again. This phase of minimal strain rate was classically termed the secondary creeping phase, but there is debate over its actual existence (Brantut et al., 2013). Tertiary creep is marked by an acceleration of strain rate after a certain amount of creep strain is reached (Baud and Meredith, 1997) leading to failure of the rock. The time from the beginning of such an experiment till the ultimate failure of the sample is termed time-to-failure t_f, and can be related to the applied load by an exponential law (Wiederhorn and Bolz, 1970)

$$t_f = t_0 e^{-b\frac{\sigma}{\sigma_0}}, \tag{1}$$

where σ is the applied load, σ_0 is the short term strength of the rock and b and t_0 are material constants of the rock. This kind of behavior is observed in many materials. It was first noted in glass and ceramics (Charles, 1958; Wiederhorn and Bolz, 1970) but later found also in natural rock material such as granite (Kranz, 1980; Kranz et al., 1982; Lockner, 1993; Masuda, 2001), sandstone (Baud and Meredith, 1997; Heap et al., 2009), limestone (Brantut et al., 2013), and basalt (Heap et al., 2011). It is likely that the behavior of time-dependent brittle creep is not restricted to these materials. However for other rock types such as shales, the necessary experimental program to obtain the t_f-σ-relationship is very tough, since the repeatability of rock strength experiments must be assured within narrow bounds.

Elastic approaches predict the wellbore wall to fail in compression by shear failure. Observations of breakouts under controlled laboratory environments however, show that tensile failure modes play an important role in the creation of breakouts (Haimson, 2007; Andersson et al., 2009). This apparent discrepancy is typically explained by coalescence of tensile microcracks leading to macroscopic failure under compressional stresses (Brantut et al., 2012, 2013). In our modeling we do not consider any particular failure mode, since brittle creep experiments are typically conducted in compression but showing evidence for tensile failure modes. However, the macroscopic observable, time-to-failure, is independent of microscopic failure modes.

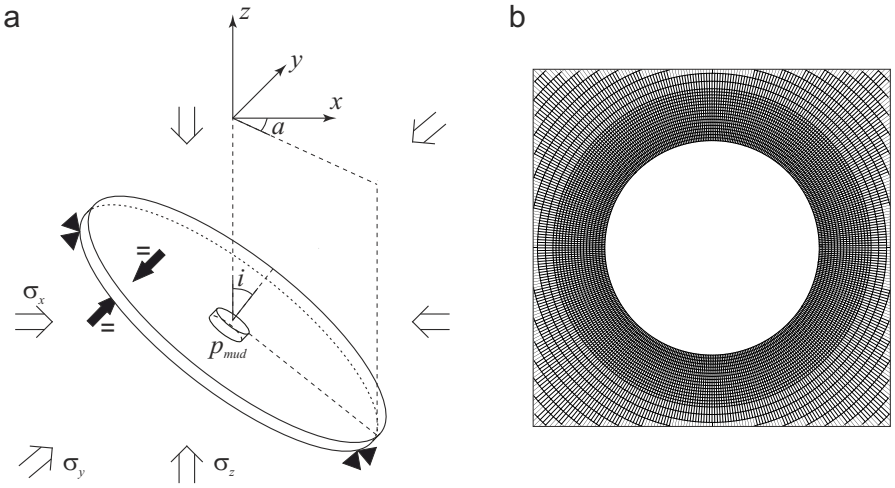

Figure 2: (a) Schematic of the FE model of a borehole with arbitrary orientation of azimuth a and inclination i, fixed displacements at the outer boundary and tied displacements of upper and lower nodes. (b) shows a closeup of the refined mesh around the wellbore.

3 Numerical Model

For our simulations we use the commercial finite element software Abaqus (Simulia), version 6.11-2. In order to compute stresses around an arbitrarily oriented wellbore we model a 3-D slice orthogonal to the wellbore axis. We apply an initial stress field at an angle to the modeled domain to take the relative orientation of the stress tensor to the wellbore into account. Boundary conditions are chosen after Ewy (1993), i.e. the outer nodes are fixed, inner nodes of the wellbore wall are free. Periodic boundary conditions along the wellbore axis are realized by tying the nodes on the top of the modeling domain to the nodes on the bottom in pairs, such that their respective displacements in all three directions are identical (Figure 2). These conditions guarantee that lines parallel to the wellbore axis remain parallel and ensure a constant thickness of the modeled volume. Yet they allow for non-planarity and warping of the modeled volume. Using these boundary conditions, the analytical solutions for stresses around an arbitrarily oriented wellbore (Fjaer et al., 2008) are matched very well. In order to simulate the effect of the weight of the drilling mud, which is used to stabilize the wellbore wall, a surface load is applied to the wellbore wall. At the beginning of the simulation the nodes at the wellbore wall are fixed to simulate the undisturbed rock. Drilling of the well is simulated by instantaneous release of this boundary condition. Additionally a radial pressure is applied to the wellbore wall representing the weight of the drilling fluid. While in principal any orientation of the wellbore can be modeled by this setup, results shown hereafter are for the case of a vertical wellbore.

To incorporate time-dependent brittle creep, we follow closely the approach developed by Amitrano and Helmstetter (2006). It bases on the assumption that time-dependent brittle creep increases the density of microcracks in a rock material. This is underpinned by numerous experiments (e.g. Heap et al., 2009), which show a remarkably congruent evolution of energy released by acoustic emission, strain and porosity changes over the time of the experiment. Increased crack density leads to degradation of the elastic moduli (Kemeny and Cook, 1986; Heap et al., 2010), thus reducing the capability of rock to support stress. Because of the degradation, stresses are redistributed increasing the load on neighboring elements. The basic constitutive behavior of the rock is modeled with linear elasticity. The time-dependent failure model is incorporated in Abaqus using a subroutine. Here the damage state of the model is read and updated according to the current stress state after each time step. The damage state of each element is described by the damage variable D, which takes the value $D = 0$ for undamaged and $D = 1$ for completely damaged states, and the consumed lifetime variable. If time-to-failure is not reached in an element, the proportion of time-to-failure which has passed in the last time step is stored and added to the consumed lifetime variable. When the time-to-failure is finally reached, damage is applied to the element by increasing D by a constant value D_0 and the consumed lifetime is reset to 0 for this element. Time increments are adjusted in each increment accounting for the time-to-failure of the element closest to failure. The numerical model is summarized in a flowchart in Figure 3.

To calculate time-to-failure we employ Equation 1. In Amitrano and Helmstetter (2006) σ is the mean major stress, which is typically the vertical stress in a uniaxial compressive test. For our wellbore environment we have almost a uniaxial stress state with σ_{rr} being the difference between formation pressure and mud pressure, thus close to zero. The hoop stress $\sigma_{\theta\theta}$ is the principal stress determining failure at the wellbore wall, thus we replace σ in Equation 1 with $\sigma_{\theta\theta}$. The hoop stress is obtained from the Cartesian stress components σ_x, σ_y and the in-plane shear stress τ_{xy}:

$$\sigma_{\theta\theta} = \frac{1}{2}\left(\sigma_x + \sigma_y\right) - \frac{1}{2}\left(\sigma_x - \sigma_y\right)\cos 2\theta - \tau_{xy}\sin 2\theta. \tag{2}$$

Input parameters are summarized in Table 1. The time-to-failure parameters t_0 and b used are taken from Masuda (2001), who conducted creep experiments on granite samples. Other rock parameters are generic but are chosen with reasonable values commonly found in the literature. We have to emphasize here, that input parameters determined from slow creep tests are not straight forward to compare with our input parameters. The experimentally obtained values for t_f are for macroscopic failure of one sample. However in our simulations, t_f is considered for microscopic failure, which accumulates to macroscopic failure only after many cycles. We neglect any effects of varying water saturation or temperature changes, although they have a large impact on the actual time-to-failure behavior of rocks (Kranz et al., 1982; Heap et al., 2009).

The degradation of Young's modulus with increasing damage has been analyzed in several studies. From cyclic compressional tests on different rock sam-

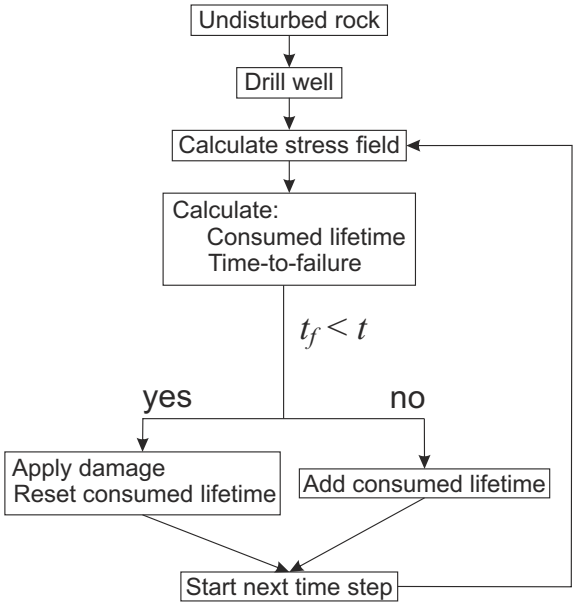

Figure 3: Flowchart of the FE simulation with time-dependent failure of single elements.

ples Heap et al. (2010) find an approximately linear decrease of the macroscopic Young's modulus with increasing crack density. Nevertheless we tested several relationships with linear, concave and convex progression of Young's modulus as a function of damage to account for the uncertainty in the actual behavior of different rock types. Here we have to differentiate between the experimentally determined values of E being macroscopic quantities lumped over the whole sample, whereas in our simulations we need to use a microscopic E valid only for each element. Therefore, we reduce E to almost zero for complete damage of $D = 1$. This is unlike the experimentally obtained macroscopic values, where E is reduced by $10 - 30\,\%$ until macroscopic failure of the sample is reached, depending on the rock type. The used relationships between Young's modulus and damage are shown in Figure 4. As is discussed below, in all simulations damage does not increase further than to where the effective Young's modulus E_{eff} is reduced to about half its original value E_0.

4 Results

Figure 5 shows the evolution of breakouts for snapshots log-spaced in time in terms of hoop stress $\sigma_{\theta\theta}$ and damage D. A gradual growth of the breakout with time is observed over the modeled period of 10^6 s (11.5 days). At the beginning, damage accumulates in a curved area adjacent to the wellbore wall. Here the

Parameter	Description	Value
Strength parameters		
t_0	TTF time factor	$2 \cdot 10^{22}$ s
b	TTF exponent	46
σ_0	uniaxial compressive strength	70 MPa
D_0	damage parameter	0.01
Elastic parameters		
E_0	initial Young's modulus	31 GPa
ν	Poisson's ratio	0.36
Stress field, effective stresses		
$\sigma_{H,\max}$	maximum horizontal stress	35 MPa
$\sigma_{h,\min}$	minimum horizontal stress	20 MPa
σ_v	vertical stress	30 MPa
p_{mud}	mud overpressure	2 MPa

Table 1: Mechanical input parameters of the numerical model.

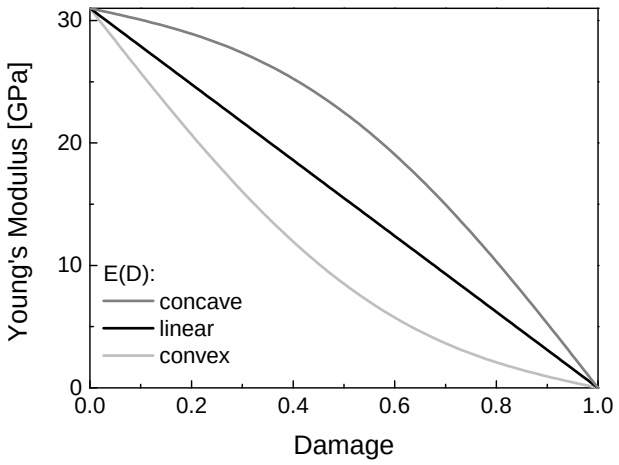

Figure 4: Relation $E(D)$ of Young's modulus E with increasing damage D for the three different models.

hoop stress decreases very strongly as time and hence damage progresses. Due to the ongoing redistribution of stress following damage, the point of maximum hoop stress moves away from the wellbore wall to the inside of the formation. With increasing deepening of the breakout, slight stress increase is observed in the vicinity of the breakout tip. In the end, a stress distribution with only small stress gradients is observed which leads to much larger t_f and hence a much slower accumulation of damage.

The evolution of the breakout dimensions in width in degrees and depth a, normalized by the wellbore radius r, is shown in Figure 6. Here, any damaged

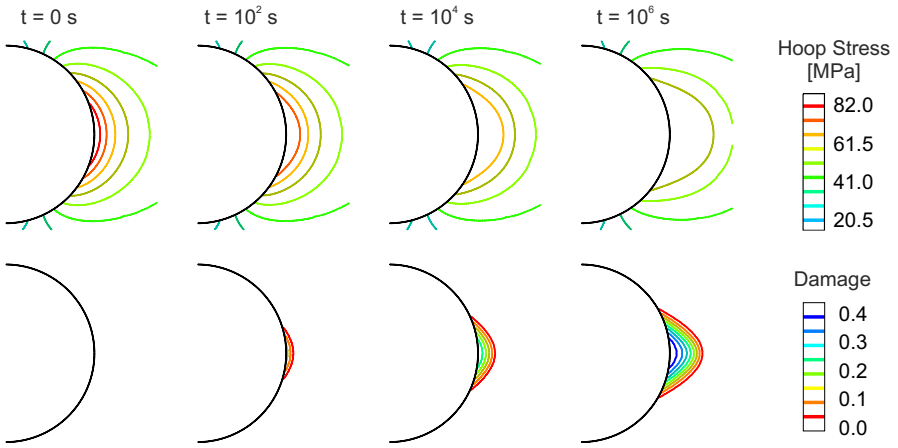

Figure 5: Evolution of hoop stress $\sigma_{\theta\theta}$ (top) and damage (bottom) over time. Note the increase of stress away from the wellbore wall.

elements are considered as part of the breakout. It is marked by a number of distinct features. At the beginning of breakout growth the shape is round with a shallow depth and an already large angular extend of around 30°. Then the breakout widens considerably to more than 60° and depth increases moderately from around $0.05\,a/r$ at the beginning to more than $0.4\,a/r$ in the end. The slope of growth in width decreases and the slope of growth in depth increases considerably when plotted in a semi-log plot as in Figure 6. Towards the end of the simulation, growth of breakouts is now mostly in depth, and width increases only moderately. Remarkable is the almost identical evolution of the breakout size for the three $E(D)$ relations. But, since breakout size was defined as the area with any damage, this is not relevant for real-world comparison. Instead, we plot the shape of the breakouts normalized by the $E(D)$ relation in terms of E_{eff} in Figure 7. We see that the shape is slightly dependent on the relation $E(D)$ with linear and convex $E(D)$ result in rounded breakouts, while for a concave $E(D)$ the breakout tip is more pronounced and the breakout takes a V-shape. Although the amount of damage in the developed breakout is very different for the $E(D)$ relations, E_{eff} is very similar for all simulations. This again underpins the robustness of our approach towards different relations for damage accumulation.

In the following, we analyze in further detail the late evolution of the breakouts coming to a stable state. For this we retrieve the event rate from the number of elements where damage was applied in one time step divided by the time increment. Figure 8 shows the evolution of event rate n over time. The log-log plot shows a power law decay of events as it is typically observed e.g. in earthquake aftershock sequences, which are commonly described by Omori's law (Utsu et al., 1995), one of the fundamental empirical relationships of seismology.

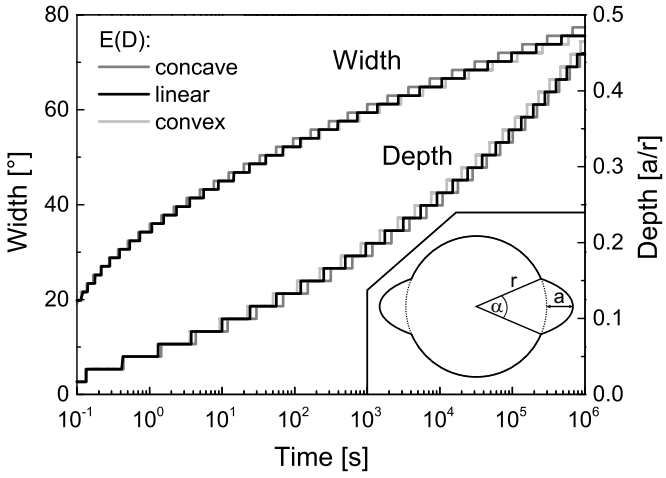

Figure 6: Growth of the breakouts for the linear and non-linear degradation relations. The width α and the depth a are used a defined in the inset. Any damaged elements are considered as part of the breakout. Up to about 10^3 s growth of the breakouts in width and depth is observed, while later the breakout growths only in depth.

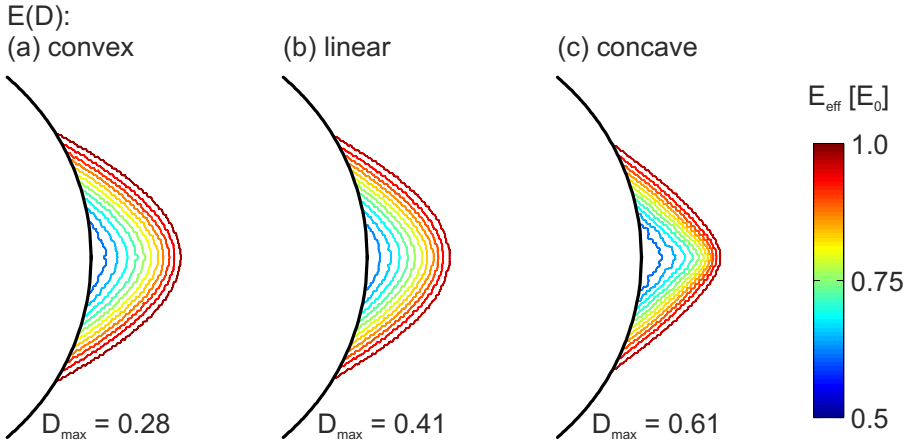

Figure 7: Shape of the breakout for different degradation relations of Young's Modulus drawn in effective Young's Moduli $E_{eff} = E(D)$.

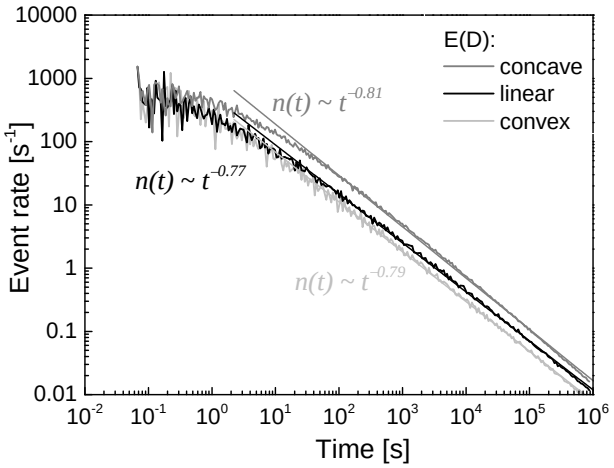

Figure 8: Decay of event rate during breakout formation for the three degradation relations along with fits of Omori's law with $c = 0$. All behave very similarly and comply with Omori's law with $p \approx 0.8$.

The modified Omori law is

$$n(t) = \frac{k}{(c+t)^p}, \tag{3}$$

where k is the amplitude of aftershock activity, c is a time offset and p is an exponent describing the decay rate. Neglecting the time offset (which is a debatable quantity related to overlapping recordings of seismicity), we fit a decay exponent p in the order of 0.77 to 0.81 to the event rate, depending on the $E(D)$ relation. These values are a bit lower than what is observed for aftershock sequences. Here values of $p = 1.0$ to 1.2 are commonly found (Shcherbakov et al., 2004) representing a faster decline of activity. Our relatively small values of p is in agreement with the numerical experiments of uniaxial compression by Amitrano and Helmstetter (2006) and suggests a slower decay of activity by the process of time-dependent brittle creep, compared to most aftershock sequences.

Laboratory experiments on uniaxially stressed samples suggest that Poisson's ratio ν increases with increasing damage and progressive stiffness degradation of E (Heap et al., 2010). We therefore checked the effect of increasing ν with increasing damage for the linear $E(D)$ relation. ν was increased linearly with damage from 0.25 for undamaged matrix to 0.5 for $D = 1$. Comparing with the result for constant ν the overall shape and size of the breakout is the same, however the areas of large damage have a slightly larger extent, both in width and depth. While the overall breakout has a round shape, the highly damaged areas take a V-shape.

For one test we solve the constitutive equations of poroelasticity (Rice and Cleary, 1976) incorporated in Abaqus instead of the elastic constitutive model.

The boundary conditions were the same, except for an additional condition for the additional degree of freedom, namely pore fluid pressure p. According to the mud pressure which is applied as surface load to the wellbore wall in all previous simulations, also pore fluid pressure is prescribed with the same value at the wellbore wall. Following the poroelastic approach, the time-to-failure criterion is evaluated using effective stresses ($\underline{\sigma}_{\text{eff}} = \underline{\sigma} - p \cdot \underline{I}$). To incorporate also the effect of increasing crack density with increasing damage on the hydraulic properties of the formation, hydraulic permeability k (in m^2) is defined exponentially dependent on the damage variable, with $\log(k) = -13$ for $D = 0$ and $\log(k) = -9$ for $D = 1$ and linearly interpolated between these values. The effect of increasing pressure solution with increasing pore fluid pressure in the rock matrix is not captured by this simplistic poroelastic model, besides there is no experimental evidence that increased pore fluid pressure, but constant effective stresses, actually enhances subcritical crack growth (Heap et al., 2009). Because of the stabilizing effect of pore fluid pressure in the rock matrix, the propagation of breakouts is slower for a poroelastic material than for an elastic material but follows the same general trend and shape. Therefore we did not study effects of poroelasticity any further.

5 Discussion

Although they are almost never considered in typical analyses of wellbore failure, there is no reason why inelastic effects such as creep and accompanied time-dependent brittle failure should be absent along the borehole wall. Haimson (2007) observed the micromechanical processes of breakout formation in different kinds of rock. For the example of Lac-du-Bonnet granite he observes successive spallation of rock flakes from the borehole wall, that leave small cantilevers of rock behind, when the rock flakes fall off. The residual strength of these small cantilevers is enough to reduce the next flakes length. Eventually this cascade of less and less damaged rock leads to stable V-shaped breakouts. Comparing to our damage mechanics approach, the formation of individual rock flakes with microcracks in between can be regarded as stiffness degradation of a damaged rock material. Thus, the progressive failure of flakes of rock, combined with the accompanied stress redistribution can be suitably analyzed by a damage mechanics approach.

The evolution of borehole breakouts show common features of seismic aftershock sequences. The drilling of the well causes large localized stress perturbations, comparable to localized stress increases following an earthquake main shock. Similar to the release of stress peaks on fault asperities, heterogeneities along the wellbore wall caused by an increased microcrack density, fail over time through the processes of stress corrosion or brittle creep (Das and Scholz, 1981). This releases localized stress peaks and eventually leads to a stable state, where stress perturbations are such that the time-to-failure grows to orders which are irrelevant for engineering processes.

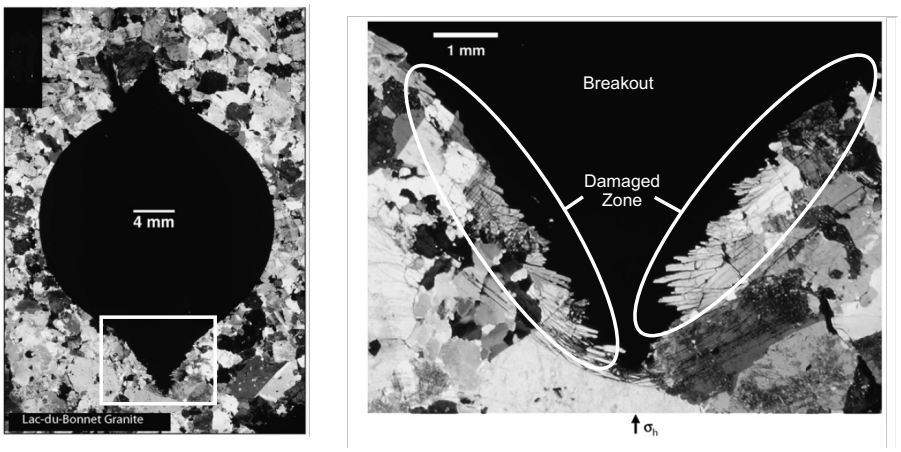

Figure 9: Breakout with dog ear-shape in a Lac-du-Bonnet granite sample created in a lab test. Adapted from Haimson (2007).

6 Conclusions

We propose a simple geomechanical model to explain the time-dependency of wellbore breakouts. Using an implementation of time-dependent brittle creep to the commercial finite element package Abaqus we are able to match several characteristics of breakout growth in time, as observed in-situ. These are a relatively quick widening of the breakouts and subsequent growth mainly in depth, leading to a distinct V-shape. Overall the evolution of the breakout size comes to a halt by an Omori-type decay of event rate. The breakout geometry resulting from the time-dependent evolution shows the typical V-shape observed in many wells. This is caused by the development of an excavation damaged zone around the wellbore and the breakout reducing stresses in damaged elements and redistributing, i.e. increasing stresses to neighboring elements. With time, stresses are redistributed more and more such, that the residual strength of the excavation damaged zone is sufficient to support the residual stresses for very long time spans and the growth of breakouts stops. When using the geometry of breakouts to infer stress magnitudes, great care must be taken that a stable state has been reached. Still then the assumptions used to predict breakout size from a given stress state need to be verified and calibrated by experiments.

Acknowledgements

The work presented was partly conducted under the project "Reduzierung der geologisch bedingten bohrtechnischen Risiken - Bohrlochstabilität in tertiären Tonsteinfolgen im Oberrheingraben als Hindernis fr die Erschließung geothermischer Reservoire" under management of Institute of Soil Mechanics and Rock

Mechanics at Karlsruhe Institute of Technology with financial support by the German Federal Ministry for the Environment, Nature Conservation and Nuclear Safety, BMU, grant agreement no. 0327599. Additional funding by EnBW Energie Baden-Württemberg AG is acknowledged.

References

Amitrano, D. and Helmstetter, A. (2006). Brittle creep, damage, and time to failure in rocks. *Journal of Geophysical Research*, 111(B11):B11201.

Anderson, O. L. and Grew, P. C. (1977). Stress corrosion theory of crack propagation with applications to geophysics. *Reviews of Geophysics*, 15(1):77.

Andersson, J. C., Martin, C. D., and Stille, H. (2009). The Äspö Pillar Stability Experiment: Part II-Rock mass response to coupled excavation-induced and thermal-induced stresses. *International Journal of Rock Mechanics and Mining Sciences*, 46(5):879–895.

Atkinson, B. K. (1984). Subcritical Crack Growth in Geological Materials. *Journal of Geophysical Research*, 89(B6):4077–4114.

Baud, P. and Meredith, P. G. (1997). Damage accumulation during triaxial creep of Darley Dale sandstone from pore volumometry and acoustic emission. *International Journal of Rock Mechanics and Mining Sciences*, 34(3-4):24.e1–24.e10.

Brantut, N., Baud, P., Heap, M., and Meredith, P. G. (2012). Micromechanics of brittle creep in rocks. *Journal of Geophysical Research*, 117(B8):B08412.

Brantut, N., Heap, M., Meredith, P., and Baud, P. (2013). Time-dependent cracking and brittle creep in crustal rocks: A review. *Journal of Structural Geology*, 52:17–43.

Brudy, M., Zoback, M. D., Fuchs, K., Rummel, F., and Baumgärtner, J. (1997). Estimation of the complete stress tensor to 8 km depth in the KTB scientific drill holes: Implications for crustal strength. *Journal of Geophysical Research*, 102(B8):18453–18475.

Charles, R. (1958). The static fatigue of glass. *Journal of Applied Physics*, 29:1549–1560.

Chen, G., Chenevert, M. E., Sharma, M. M., and Yu, M. (2003). A study of wellbore stability in shales including poroelastic, chemical, and thermal effects. *Journal of Petroleum Science and Engineering*, 38:167–176.

Cornet, F. H., Bérard, T., and Bourouis, S. (2007). How close to failure is a granite rock mass at a 5 km depth. *International Journal of Rock Mechanics and Mining Sciences*, 44(1):47–66.

Das, S. and Scholz, C. H. (1981). Theory of time-dependent rupture in the Earth. *Journal of Geophysical Research*, 86(B7):6039–6051.

Detournay, E. and Cheng, A. H. D. (1988). Poroelastic response of a borehole in a non-hydrostatic stress field. *International Journal of Rock Mechanics and Mining Sciences & Geomechanics Abstracts*, 25(3):171–182.

Ewy, R. T. (1993). Yield and closure of directional and horizontal wells. *International Journal of Rock Mechanics and Mining Sciences & Geomechanics Abstracts*, 30(7):1061–1067.

Fjaer, E., Holt, R. M., Horsrud, P., Raaen, A. M., and Risnes, R. (2008). *Petroleum Related Rock Mechanics*. Elsevier.

Gran, J. D., Rundle, J. B., and Turcotte, D. L. (2012). A possible mechanism for aftershocks: time-dependent stress relaxation in a slider-block model. *Geophysical Journal International*, 191(2):459–466.

Haimson, B. C. (2007). Micromechanisms of borehole instability leading to breakouts in rocks. *International Journal of Rock Mechanics and Mining Sciences*, 44(2):157–173.

Haimson, B. C. and Chang, C. (2002). True triaxial strength of the KTB amphibolite under borehole wall conditions and its use to estimate the maximum horizontal in situ stress. *Journal of Geophysical Research*, 107(B10):2257.

Heap, M., Baud, P., Meredith, P. G., Bell, A. F., and Main, I. G. (2009). Time-dependent brittle creep in Darley Dale sandstone. *Journal of Geophysical Research*, 114(B7):B07203.

Heap, M., Baud, P., Meredith, P. G., Vinciguerra, S., Bell, A. F., and Main, I. G. (2011). Brittle creep in basalt and its application to time-dependent volcano deformation. *Earth and Planetary Science Letters*, 307(1-2):71–82.

Heap, M., Faulkner, D. R., Meredith, P. G., and Vinciguerra, S. (2010). Elastic moduli evolution and accompanying stress changes with increasing crack damage: implications for stress changes around fault zones and volcanoes during deformation. *Geophysical Journal International*, 183(1):225–236.

Hiramatsu, Y. and Oka, Y. (1968). Determination of the stress in rock unaffected by boreholes or drifts, from measured strains or deformations. *International Journal of Rock Mechanics and Mining Sciences & Geomechanics Abstracts*, 5(4):337–353.

Kemeny, J. and Cook, N. G. W. (1986). Effective moduli, nonlinear deformation and strength of a cracked elastic solid. *International Journal of Rock Mechanics and Mining Sciences & Geomechanics Abstracts*, 23(2):107–118.

Kessels, W. (1989). Observation and interpretation of time-dependent behaviour of borehole stability in the Continental Deep Drilling pilot borehole. *Scientific Drilling*, 1:127–134.

Kirsch, G. (1898). Die Theorie der Elastizität und die Bedürfnisse der Festigkeitslehre. *Zeitschrift des Vereins Deutscher Ingenieure*, 42:797–807.

Kranz, R. L. (1980). The effects of confining pressure and stress difference on static fatigue of granite. *Journal of Geophysical Research*, 85(B4):1854–1866.

Kranz, R. L., Harris, W. J., and Carter, N. L. (1982). Static fatigue of granite at 200 C. *Geophysical Research Letters*, 9(1):1–4.

Lee, M. and Haimson, B. C. (1993). Laboratory study of borehole breakouts in Lac du Bonnet granite: a case of extensile failure mechanism. *International Journal of Rock Mechanics and Mining Sciences & Geomechanics Abstracts*, 30(7):1039–1045.

Lockner, D. A. (1993). Room temperature creep in saturated granite. *Journal of Geophysical Research*, 98(B1):475–487.

Lockner, D. A. (1998). A generalized law for brittle deformation of Westerly granite. *Journal of Geophysical Research-Solid Earth*, 103(B3):5107–5123.

Masuda, K. (2001). Effects of water on rock strength in a brittle regime. *Journal of Structural Geology*, 23:1653–1657.

Moore, J. C., Chang, C., McNeill, L., Thu, M. K., Yamada, Y., and Huftile, G. (2011). Growth of borehole breakouts with time after drilling: Implications for state of stress, NanTroSEIZE transect, SW Japan. *Geochemistry Geophysics Geosystems*, 12:Q04D09.

Rice, J. R. and Cleary, M. P. (1976). Some basic stress diffusion solutions for fluid-saturated elastic porous media with compressible constituents. *Reviews of Geophysics and Space Physics*, 14(2):227–241.

Rutter, E. H. (1976). Kinetics of rock deformation by pressure solution. *Philosophical Transactions of the Royal Society of London Series a-Mathematical Physical and Engineering Sciences*, 283(1312):203–219.

Scholz, C. H. (1968). Mechanism of creep in brittle rock. *Journal of Geophysical Research*, 73(10):3295.

Shcherbakov, R., Turcotte, D. L., and Rundle, J. B. (2004). A generalized Omori's law for earthquake aftershock decay. *Geophysical Research Letters*, 31(11):L11613.

Triantafyllidis, T., Kreuter, H., Mutschler, T., Schoenball, M., Tembe, S., Rübel, S., Osan, C., Balthasar, K., Wenke, A., and Sperber, A. (2010). Reduzierung der geologisch bedingten bohrtechnischen Risiken Bohrlochstabilität in tertiären Tonsteinfolgen im Oberrheingraben. Technical report, Grant no. 0327599, Institute of Soil Mechanics and Rock Mechanics, Karlsruhe Institute of Technology.

Utsu, T., Ogata, Y., and Matsuura, R. S. (1995). The centenary of the Omori formula for a decay law of aftershock activity. *Journal of Physics of the Earth*, 43(1):1–33.

Vernik, L., Zoback, M. D., and Brudy, M. (1992). Methodology and application of the wellbore breakout analysis in estimating the maximum horizontal stress magnitude in the KTB pilot hole. *Scientific Drilling*, 3:161–169.

Wiederhorn, S. M. and Bolz, L. H. (1970). Stress corrosion and static fatigue of glass. *Journal of The American Ceramic Society*, 50:543–548.

Xu, T., Tang, C., Zhao, J., Li, L., and Heap, M. (2012). Modelling the time-dependent rheological behaviour of heterogeneous brittle rocks. *Geophysical Journal International*, 189(3):1781–1796.

Zang, A. and Stephansson, O. (2010). *Stress Field of the Earth's Crust*. Springer.

Zoback, M. D., Barton, C. A., Brudy, M., Castillo, D. A., Finkbeiner, T., Grollimund, B. R., Moos, D. B., Peska, P., Ward, C. D., and Wiprut, D. J. (2003). Determination of stress orientation and magnitude in deep wells. *International Journal of Rock Mechanics and Mining Sciences*, 40(7-8):1049–1076.

Zoback, M. D., Moos, D., Mastin, L., and Anderson, R. N. (1985). Well bore breakouts and in situ stress. *Journal of Geophysical Research*, 90(B7):5523–5530.